ORGANIC PROCESS RESEARCH & DEVELOPMENT
OPR&D

pubs.acs.org/OPRD

Article

Real-Time Monitoring of Continuous Pharmaceutical Mixed Suspension Mixed Product Removal Crystallization Using Image Analysis

András Domokos, Lajos Madarász, György Stoffán, Kornélia Tacsi, Dorián Galata, Kristóf Csorba, Panna Vass,* Zsombor K. Nagy, and Hajnalka Pataki

Cite This: *Org. Process Res. Dev.* 2022, 26, 149−158

Read Online

ACCESS | Metrics & More | Article Recommendations

ABSTRACT: In this work, we developed an in-line image analysis system for the monitoring of the continuous crystallization of an active pharmaceutical ingredient. Acetylsalicylic acid was crystallized in a mixed suspension mixed product removal crystallizer, which was equipped with overflow tubing as an outlet. A steep glass plate was placed under the outlet onto which the slurry dripped on its surface. The glass plate spread and guided the droplets toward the product collection filter. A high-speed process camera was mounted above the glass plate to capture images of the crystals. Several light sources were tested in various positions to find the appropriate experimental setup for the optimal image quality. Samples were taken during continuous operation for off-line particle size analysis in order to compare to the crystal size distributions calculated from the images. The results were in good agreement, and the trends of the process could be followed well using the images. As a next step, image analysis was operated throughout the entire continuous crystallization experiment, and a huge quantity of information was collected from the process. The crystal size distribution of the product was calculated every 30 s, which provided a thorough and detailed insight into the crystallization process.

KEYWORDS: *continuous crystallization, image analysis, process analytical technology, MSMPR*

1. INTRODUCTION

Although continuous manufacturing (CM) has several advantages, the pharmaceutical industry still relies mainly on traditional batch processes.[1] When the existing batchwise technologies are replaced with CM, faster, cheaper, more flexible, and safer production can be developed.[2−4] In order to reach the productivity of the existing batch procedures, it is necessary to operate a smaller scale continuous system for longer periods or even without stoppage. During operation, a steady state can be reached, when process parameters and product quality are constant at the different locations of the manufacturing line. Thus, real-time monitoring and control of the production is significantly easier compared to the continuously changing nature of conventional batch processes. With this new approach, very consistent product quality can be achieved.[5] Realizing the mentioned benefits of moving from batch to CM, the Food and Drug Administration (FDA) published the concept of Process Analytical Technologies (PAT) and Quality by Design (QbD) in the 2000s.[6] These initiatives promote the adaption of CM techniques coupled with in-line analytical tools for enhanced quality control (QC).[7]

Crystallization in the pharmaceutical industry is fundamental for the separation and purification of the synthesized active pharmaceutical ingredients (APIs).[8] The properties of the crystal product, i.e., size, shape, or morphology, have a great impact on the following filtration, granulation, blending, and tableting steps.[9] Also, the dissolution and bioavailability of the final drug product can be affected through these material attributes.[10] Consequently, monitoring of crystallization to control the crystal size and shape is of utmost importance.[11,12] The significance of the process drew attention to continuous crystallization in recent years, and it became one of the most intensively studied areas of continuous pharmaceutical technologies.[13,14] The most commonly applied device in the research studies is the mixed suspension mixed product removal (MSMPR) crystallizer.[15]

The crystal size distribution (CSD) is often analyzed by laser diffraction or sieve analysis.[12] Nevertheless, these off-line techniques do not provide information about the shape of the particles. Also, in-line measurement is required for the more accurate real-time monitoring of the process. In-line sensors, such as focused beam reflectance measurement (FBRM) and three-dimensional optical reflectance measurement (3D-ORM), can be applied for this purpose.[16] FBRM and 3D-ORM measure the chord length distribution (CLD) of the crystals, which is related to the size and shape of the particles. However, the deduction of the actual CSD and shape from the experimental CLD data is challenging.[17]

Received: September 28, 2021
Published: December 29, 2021

Image analysis is another possible technique for the in-line monitoring of crystallization processes.[18] This technique has many advantages over other methods since it could provide abundant information not just about crystal size but also regarding crystal morphology, degree of agglomeration, or suspension density.[19] Known examples for image analysis-based techniques are particle vision and measurement (PVM),[20,21] bulk video imaging (BVI),[22,23] or the application of a flow-through cell with an external camera.[24,25] Nevertheless, these by themselves are usually only suitable for qualitative analysis, since the crystals are often captured partially or completely out of focus and overlapping with each other.[9,26] For the reliable quantification of crystal size and shape, the mentioned techniques are usually applied in combination with other measurement tools.[9,16,27−30]

In order to apply image analysis for accurate process monitoring, novel approaches were developed to extract quantitative information from the captured images. Complex algorithms were reported with which the pictures taken with PVM probes could provide information about the particle size.[9,20,26,31,32] El Arnaout et al. presented a novel immersed image analysis probe and applied it for the monitoring of batch crystallizations.[33,34] An invasive image analysis method was developed by Lu et al., which was applied for in-line morphology identification and agglomeration segmentation during the cooling batch crystallization of L-glutamic acid.[35] 2D/3D imaging devices and algorithms were developed for various types of crystal products for improved crystal size and shape analysis.[36−40] Hou et al. applied two external cameras during the batch crystallization of L-glutamic acid to obtain 3D CSD.[37] Microcomputed tomography was used to obtain 3D images of potash alum crystals for morphological characterization by Schiele et al.[40] Neoptolemou et al. proposed a novel 2D imaging technique to characterize overlapping needle-like crystals.[39] Crystallization reactors coupled with flow through cells and microscopic systems were also used for particle measurement by image analysis.[25,36,41,42] A few examples can be found for the application of deep learning and neural networks to acquire real-time particle size distributions (PSDs) during batch crystallizations.[19,43−45]

As it could be seen, accurate and reliable image analysis systems were developed for the in-line monitoring of batch crystallizations. Meanwhile, only a handful of examples can be found for the image analysis-based monitoring of continuous crystallization processes.[24,46−50] Among these, only Capellades et al. used MSMPR reactors, which is the most widespread continuous crystallization system.[49] They developed an image analysis method for the quantitative determination of crystal size and shape using an optical microscope equipped with a high-definition camera and an image processing software (ImageJ). However, their approach was the off-line measurement of diluted samples taken from the suspension with which accurate and continuous in-line real-time process monitoring was not feasible.

Recently, we built a novel dynamic image analysis (DIA) videometric system based on a high-speed camera coupled with an in-house developed software capable of processing several hundred images per second. This technique was first applied for the real-time monitoring of twin-screw wet granulation[51] and for the feedback control of powder feeding.[52] The main goal of this work was to extend the applicability of the DIA system for the real-time in-line monitoring of a continuous MSMPR crystallization process. The previously published setup for the continuous crystallization of acetylsalicylic acid (ASA) from a flow reaction mixture[53,54] was modified to allow the application of real-time monitoring with the camera. Different camera and illumination arrangements were tested to obtain pictures with the best quality. Samples were taken from the continuously crystallized product for conventional off-line analysis, and the results were compared to image analysis. The process was operated for longer to reach steady state, and the trends in CSD were followed by DIA throughout the entire experiment.

2. EXPERIMENTAL MATERIALS AND METHODS

2.1. Materials. Acetylsalicylic acid (ASA) (>99%) and salicylic acid (SA) (>99%) were obtained from Merck (Budapest, Hungary). Lab grade ethyl acetate (EtOAc), ethanol (EtOH), acetic acid (AcOH), phosphoric acid (H_3PO_4) (85 wt %), and heptane were purchased from Sigma-Aldrich (Budapest, Hungary).

Microcrystalline cellulose (Retsch GmbH, Haan, Germany) pellets were produced in-house for the comparison of the different applied particle size measurement techniques. 300 and 500 μm mesh sieves were used to sift the pellets.

2.2. Continuous Crystallization Setup and Procedure. The continuous crystallization experiments were carried out with the experimental setup presented in a previous study by the authors (Figure 1), supplemented with the image analysis

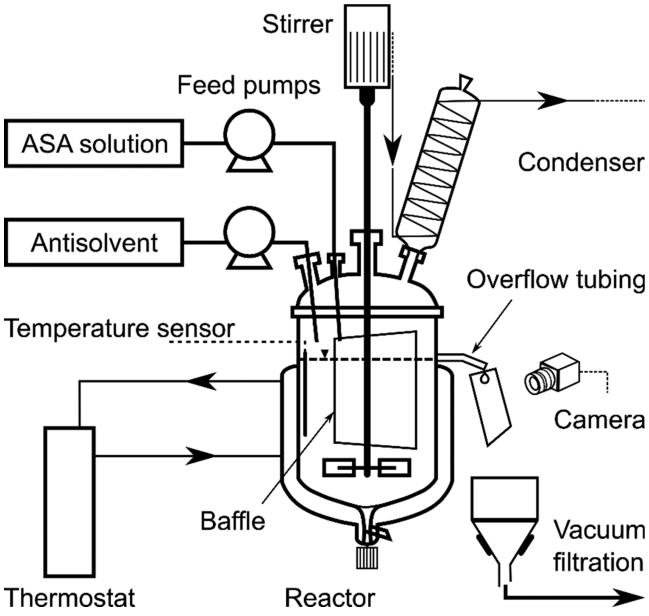

Figure 1. Schematic image of the experimental setup. Modified from ref 53. Copyright 2020 American Chemical Society.

system.[53] A 250 mL jacketed glass reactor (DN 60, Schmizo, Switzerland) was used. Overhead stirring was provided by a Eurostar power control-visc type stirrer (IKA, Germany) with a PTFE-coated Ruston 6-blade impeller. The temperature inside the crystallizer was monitored by a Pt-100 thermometer, and a Huber Ministat 230 monofluid thermostat was applied for temperature control. The MSMPR reactor was equipped with overflow tubing for product withdrawal. Thus, the outlet flow of the suspension was continuous and equivalent to the inlet feeding rate. A PTFE vertical baffle plate was also placed in the reactor to separate the feeding from product removal

https://doi.org/10.1021/acs.oprd.1c00372
Org. Process Res. Dev. 2022, 26, 149−158

and to ensure the uniform residence time distribution of the crystals. The crystals had to dive under the baffle to reach the overflow tubing. The suspension was agitated at 700 rpm to avoid the sedimentation of the crystals. The temperature was set to 0 °C during the experiments.

The detailed MSMPR crystallization setup was supplemented with an image analysis system in this study: a glass plate was positioned under the end of the overflow tubing onto which the outlet suspension was dripping and guided down into a glass filter used for crystal collection. The images for particle size analysis were recorded while flowing down on this glass plate by placing a high-speed camera above it. For more details about the image analysis setup, see Section 2.3.

The continuous crystallization of ASA was carried out from the reaction mixture of the flow synthesis of the API.[53−55] The composition of the final reaction mixture is presented in Table 1. The API solution for the crystallization experiments

Table 1. Composition of 1000 mL of the Flow Reaction Mixture Containing ASA

material	quantity
acetylsalicylic acid	97.61 g
salicylic acid	5.14 g
ethyl acetate	794.61 mL
acetic acid	163.26 mL
ethanol	38.25 mL
phosphoric acid (85%)	3.90 mL

modeling the flow reaction mixture was prepared according to this recipe prior to the experiments, typically in a quantity of 1000 mL. Heptane was used as the antisolvent during the process in a volumetric ratio of 4:1.

At the beginning of the experiments, 40 mL of heptane was poured in the empty reactor, which was thermostated at 0 °C. Ten mL of the reaction mixture was pipetted to the agitated heptane to create a starting suspension. The ASA and the heptane streams were fed into this starting suspension. The reaction mixture was fed by a Jasco PU-980 pump, and a Syrris Asia syringe pump was applied for dosing the antisolvent. During the experiments, the temperature (T) was set to 0 °C and the residence time (τ) was 25 min. Thus, the flow rates of the ASA and the heptane streams were 2 and 8 mL/min, respectively. The product slurry flowed out through the overflow and dripped onto a glass plate in front of which a camera was positioned for process monitoring (for more details, see Section 2.3) (Figure 1). Under the glass plate, the slurry was directly filtered using G2 or G3 glass filters for product collection. Samples were taken at each residence time for off-line analysis by collecting the product in separate filters.

2.3. Imaging Setup and Image Analysis Software. A steep, almost vertical glass plate (10 × 5 cm) was positioned under the overflow tubing outlet of the reactor. The angle of inclination was set manually before each experiment to aim the dripping suspension to the top of the glass plate. Thus, the suspension could spread on its surface while flowing down. A Basler acA1920-155um high-speed camera (Basler AG, Ahrensburg, Germany) was mounted above the lower section of the glass plate to take images of the crystals for analysis. The camera was equipped with a standard microscope lens with 4× magnification. The surface of the glass was silanized in order to reduce the sticking of the particles to the plate. The experimental setup is presented in Figure 1. The process camera was operated at 100 frames per second (fps) with a resolution of 1920 × 1200 and 250 μs exposure time. Several illumination devices and arrangements were tested (see Section 3.2). For the final experimental setup, a BEL Halogen fiber optic illuminator was chosen, which had two independently adjustable light sources at the end of the metal pipes (90673, BEL, China) (Figure 2). Illumination was positioned behind the glass plate facing the camera (see Section 3.2).

Figure 2. BEL Halogen illuminator used for in-line real-time image analysis in the final continuous crystallization experimental setup.

Images of the flowing crystals were analyzed using a custom image analysis software written in C++ programming language by the authors using the OpenCV application programming interface.[56] The communication with the graphical user interface was written in C#. During the process, after an image was captured and read from the camera, the following image processing steps were applied: Gaussian blur → Thresholding (Binarization) → Contouring (Edge detection) (Figure 3).

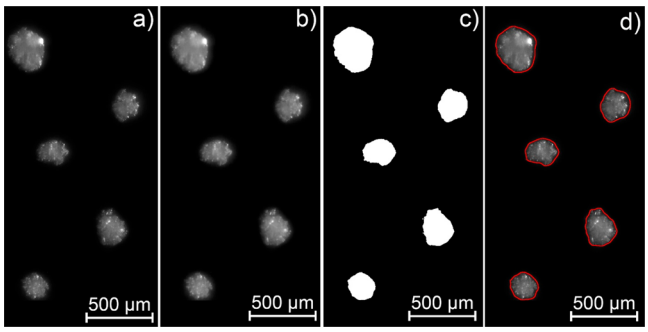

Figure 3. Stages of image processing: (a) cropped segment of raw image; (b) Gaussian blur; (c) thresholding; (d) contouring.

The particle size was determined from the contours by calculating the mean of the minimum and maximum Feret diameters (also referred to as caliper diameters) (Figure 4).

Certain particles were recorded multiple times due to the periodic dripping of the slurry droplets. In order to reduce the bias of the PSD because of these crystals, a particle tracking algorithm was also implemented into the image analysis software. This algorithm tracked the size and centroid of each particle present in consecutive images by which multiple occurrences could be eliminated. During the continuous crystallization experiments, the camera was operated continuously with 100 fps, and the pictures captured during the time period of the off-line sampling were saved separately. Thus, the

https://doi.org/10.1021/acs.oprd.1c00372
Org. Process Res. Dev. 2022, 26, 149−158

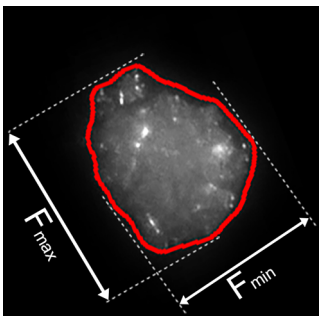

Figure 4. Visual representation of the minimum and maximum Feret diameters.

result of off-line CSD analysis could be compared to the image analysis of the same crystals. The volumetric distribution value D_v50 was applied to characterize the CSD of the products along with the direct comparison of the distributions.

2.4. Validation of the Camera-Based System. The particle size measurement capability of the developed camera-based DIA system was tested and validated by comparing it to other, more conventional particle sizing techniques: Malvern Mastersizer (Malvern Instruments, Worchestershire, UK) and Parsum IPP-70 probe (Parsum GmbH, Germany). The methods were compared via the analysis of MCC pellet samples produced in-house and sifted using 300 and 500 μm mesh sieves to obtain narrow particle size distributions.

The particle size measuring principle of the Parsum probe is spatial filtering velocimetry (SFV), while the Malvern Mastersizer applies standard laser diffraction. The Malvern Mastersizer calculates particle size via equivalent spherical diameter, and the Parsum determines particle chord length, while our imaging system determines the mean of the maximum and minimum Feret diameters. For the tests, we used highly spherical pellets, thus minimizing the effect of how the different equipment treat the particle shape. Additionally, the MCC pellets were quite stable, and almost no particle breakage could be observed even after multiple measurements.

The samples could be fully retrieved from the SFV and the camera-based measurements but not from the Mastersizer. Accordingly, the measurement order for each sample was Camera → Parsum → Malvern with sample recollection between the measurements. This way, the same material could be measured with the different methods. During the imaging and the Parsum measurements, a vibratory feeder equipped with a V-shaped chute was used to feed the samples into the measuring equipment. In order to avoid overlapping of the particles, the feeder was set to 10% intensity.

2.5. Microscope Imaging. The crystal size and habit of the samples was investigated by using a CKX53 inverse microscope equipped with an 18Mp CAM-SC180 Camera set with a magnification of 4×. Before analysis, the crystals were dispersed in silicone oil.

2.6. Off-Line Particle Size Measurements. The PSD of the crystals was measured off-line using the Parsum IPP 70-s particle sizing probe in batch mode. The samples were dispersed into the Parsum probe for estimating the chord length of the crystals. For the tests, 3 MPa air pressure was applied, and the number of the measured particles was ca. 2500 in each sample for reliable measurement results. For the comparison of the results, either the entire PSD or the D_v10, -50, and -90 values of the distributions was/were plotted. (On the basis of earlier results with this crystallization system, the Malvern Mastersizer was not suitable to measure the PSD of the crystals accurately and reproductively. Thus, the Malvern Mastersizer was only used during the validation of the DIA system.)

3. RESULTS AND DISCUSSION

At the beginning of the work, we validated the camera-based DIA system by analyzing the in-house produced MCC pellets with image analysis and comparing it to commonly used particle sizing reference techniques: a Parsum IPP70-S probe and a Malvern Mastersizer 2000. Next, the DIA system was installed in our continuous crystallization setup to capture real-time images of the outlet crystal suspension. Finally, the camera-based particle size measurement method was operated during the continuous crystallization procedure, and the results were evaluated.

3.1. Validation of the Camera-Based System. The MCC pellets were divided into ca. 5 g samples after sieving. The PSD of the particles was measured consecutively by DIA, Parsum, and Malvern by recollecting the same material after the first two methods. For the 3 measured samples, the obtained D_v50 values are presented in Table 2, and the distributions are shown in Figure 5.

Table 2. Particle Size Results of the MCC Pellets Obtained via Image Analysis, Parsum Probe, and Malvern Mastersizer

	particle size (D_v50, μm)		
sample no.	camera	Parsum	Malvern
1	431.9	425.6 (−1.46%)	438.2 (+1.46%)
2	439.2	420.7 (−4.21%)	444.6 (+1.23%)
3	452.0	433.4 (−4.12%)	457.9 (+1.31%)

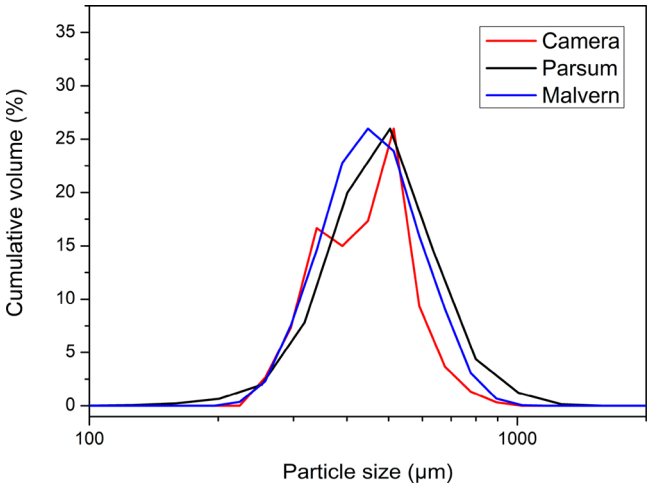

Figure 5. Measured PSDs of the MCC pellets. Each curve represents the average of the three measured samples.

As it can be seen in Figure 5 and Table 2, the measured D_v50 values show <5% difference compared to the two reference methods, and the distributions show very good similarities. According to these results, the camera-based system has a very promising applicability in the analyzed particle size range for the real-time analysis of crystal size during continuous crystallization.

https://doi.org/10.1021/acs.oprd.1c00372
Org. Process Res. Dev. 2022, 26, 149−158

3.2. Optimization of Experimental Setup: Illumination Options. As it can be seen in the Introduction, one of the main challenges of accurate and reliable crystallization monitoring with image analysis is to capture images with quality high enough for real-time PSD calculation. With immersed probes and external cameras focusing on the crystals being a difficult task and in the case of flow through cells, the clogging of transfer lines proposes substantial risks. Our MSMPR crystallizer was equipped with overflow tubing, which provided a unique opportunity to create a novel setup for image analysis without these challenges. Furthermore, although the detection is executed outside of the reactor, the CSD of the crystal suspension inside the crystallizer can be detected reliably because of the representative product removal.

We positioned a steep, almost vertical glass plate under the end of the overflow tubing. The product suspension dripped on the top of it and flowed down to the bottom under which glass filters were placed to filter and collect the crystals. The steepness of the glass plate facilitated the crystals to flow down fast, within 1 s; thus, no product accumulation occurred on the plate. On the other hand, it meant that a very short time interval was available to capture the crystals without blurring. We found that by setting the exposure time to 300 μs or higher no sharp particles could be captured. However, with short exposure times (<300 μs), very low amounts of light could enter the detector of the camera, producing low contrast in the images. In order to use the pictures for accurate particle size calculation, the contrast between the crystals and the background needed to be as high as possible. Thus, in order to improve the brightness of the crystals, external illumination was required. For this purpose, several light sources were tested in various arrangements.

The most basic ways for illumination are from behind the camera or placing the light source in front of it, as it was applied in our previous studies.[51,52] We tested a LED panel (8 W) and a LED ring (144 LEDs, 9 W) separately and together as well by placing them in front of and behind the glass plate. Unfortunately, neither of these options turned out to provide pictures of the required quality. The third illumination device was a fiber optic illuminator with two light sources at the end of independently adjustable flexible rods (ca. 60 W). With this, several variations were tested for the arrangement, and at the end, we found a position where pictures of very high quality could be obtained with an almost completely black background and white crystals. The pipes were placed behind the glass plate and rotated a little sideways at an angle, so the mean light beams crossed each other in front of the camera in the plane of the glass plate and did not face it directly. With this setup, the microscope lens was 4−5 cm from the glass plate, and the light sources were rotated to ca. 40° from the plane of the plate (Figure 6). The contrast of the white crystals and the black background was sharp, and the exposure time could be decreased to 250 μs. A few examples of the illumination options are presented in Figure 6, including the final version of the experimental setup.

3.3. In-Line and Off-Line Monitoring of Continuous Crystallization. The continuous MSMPR crystallization of ASA was carried out using the experimental setup presented in Figure 1 by setting T = 0 °C and τ = 25 min. The process was operated for 10 residence times, and samples were taken from the product at each residence time for off-line analysis using the Parsum particle measurement probe and optical microscopy. (As it was mentioned in Section 2.6, in earlier studies, we found the Malvern Mastersizer inapplicable for the reliable and reproducible measurement of the PSD of the crystal product; thus, it was only used for the validation of the camera-based system.) Meanwhile, the process camera mounted above the glass plate was operated while the samples were taken, capturing pictures of the same crystals collected for off-line analysis. This way, the results of the in-line and off-line CSD measurement were well comparable. The D_v50 values obtained from the two measurements are presented in Figure 7.

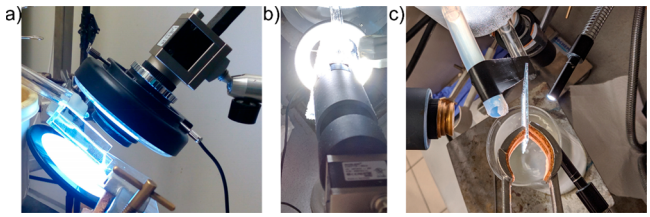

Figure 6. Pre-experimental trials for the proper arrangement of the illumination of image analysis: (a) both in front of and from behind the camera, (b) one circular light source in front of the camera, and (c) the optimal setup in which two flexible light sources were placed behind the glass plate, positioned a little sideways and askew.

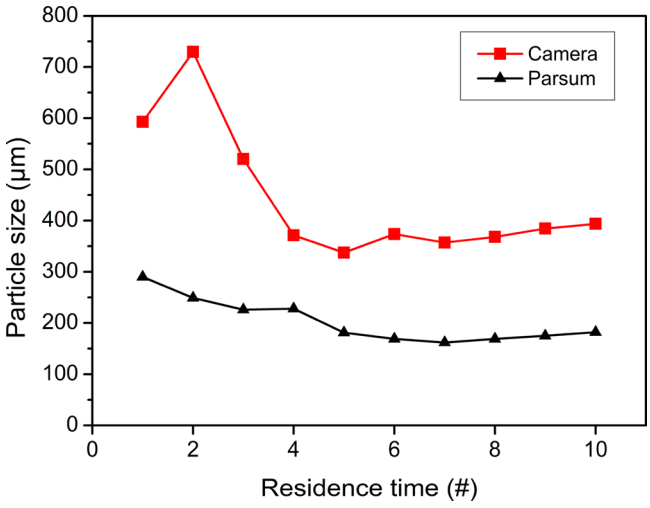

Figure 7. D_v50 values of the samples taken at each residence time of the continuous crystallization experiment measured by Parsum probe and image analysis.

According to the trends visible in Figure 7, at the beginning of the process, the two different particle size analysis techniques measured quite different D_v50 values. After reaching the fourth sample, the camera- and the Parsum-based methods became more similar, reflecting the same trend. However, there remained a substantial difference in the D_v50 values measured with the different particle sizing equipment compared to the MCC pellets. The main reason of this phenomenon is that the off-line analysis was conducted after the filtration and drying of the samples, and the crystals were dispersed with pressurized air, which might affect the crystal size. Moreover, it must also be noted that the two methods treat particle shape differently, and the measurement principle is different as well. This phenomenon has been recognized in several publications as well, dealing with the comparison of DIA-, SFV-, and laser diffraction-based particle size analysis techniques.[57,58] Thus, in the following section, the observations during the continuous crystallization experiment will be

https://doi.org/10.1021/acs.oprd.1c00372
Org. Process Res. Dev. 2022, 26, 149−158

evaluated without the Parsum results, using only DIA and optical microscopy.

After the nucleation started at the beginning of the process, the first crystals in the system were small and elongated (Figure 8b,c). Unfortunately, these tangled with each other

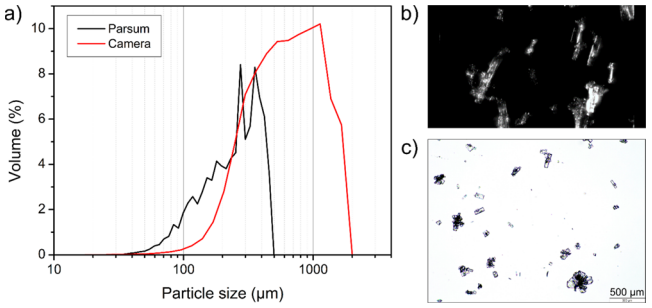

Figure 8. (a) Crystal size distribution, (b) camera-captured image of the crystals, and (c) the optical microscope image of the crystal sample taken at the first residence time of the continuous crystallization.

while flowing down on the glass plate. By manually checking the analyzed pictures, it was revealed that the algorithm could not distinguish these particles well enough, which resulted in an inaccurate CSD calculation. Compared to the off-line Parsum measurement and the scale of the microscopic picture as well, the mean crystal size was significantly bigger (Figure 8).

As the process proceeded, crystal growth and agglomeration took place, and these bigger particles were flowing down on the glass plate in front of the camera becoming increasingly distinguishable from each other. Also, the transparency of the agglomerates was much lower than at the beginning of the process, improving the accuracy of DIA (Figure 9b). After reaching the third residence time, the shape of the CSD obtained from the image analysis was very similar to the off-line result, and the difference of the mean crystal size decreased too (Figure 9a).

Due to the intensive agitation, after the agglomerated particles reached a certain size, secondary nucleation was initiated, resulting in a bimodal CSD in the fourth sample (Figure 10a,b), which was also slightly visible in the fifth sample (Figure 10c,d). The difference between the mean crystal size result of the two applied methods further decreased at these samples, and the formed bimodality and its disappearance could be detected by both techniques.

Following approximately the sixth residence time, a steady state was reached and the CSD of the product became unimodal, since almost identical CSDs were obtained from here until the end of the experiment (Figure 11a). The quality of the images captured during this period was very good, resulting in an accurate and reproducible DIA measurement (Figure 11b). According to the scale of the optical microscope image, the DIA-measured PSD was very accurate and reliable. The difference between the mean crystal size measured by the two methods did not disappear completely.

In conclusion, the continuous crystallization process could be accurately monitored by DIA. The events of the process were similarly well detectable by using the captured pictures (agglomeration, breakage, stabilization of steady state with slight further agglomeration). Further improvements would be required to address the size difference of the methods; however because of the different measurement principles of the techniques, it cannot be eliminated completely. As it has been shown in the literature as well, even in the case of spherical particles, the different, well-known particle size measurement tools provide slightly different average particle sizes.[12] Another conclusion is that the CSD obtained by Parsum was significantly less smooth and much noisier. The origin of this phenomenon is that during the Parsum measurements ~2500 particles were measured from each sample, while the pictures captured during the sampling time interval (4 min) contained typically over one million crystals. This makes DIA faster and much more reliable.

3.4. Real-Time Continuous Monitoring with DIA.

Following the sampling-based comparison of the developed DIA method to the conventional off-line particle size measurement, it was found that our technique was capable of reliably and accurately monitoring the trends of continuous crystallization. As a step forward, instead of taking pictures only during the intervals of sampling, we attempted to implement the continuous in-line monitoring of the crystallization throughout the entire operation. This way, a deeper process understanding was possible and events occurring between sampling times could be detected immediately.

During the experiment, the same conditions were applied for the continuous crystallization of ASA; thus, the results could be compared to the previously detailed experiment (T = 0 °C, τ = 25 min). The process was initiated in the same way (see Section 2.2), and the operation of the camera used for image analysis was started when the product slurry began to flow out of the reactor through the overflow tubing. As we experienced in the previous experiment, a huge quantity of data was

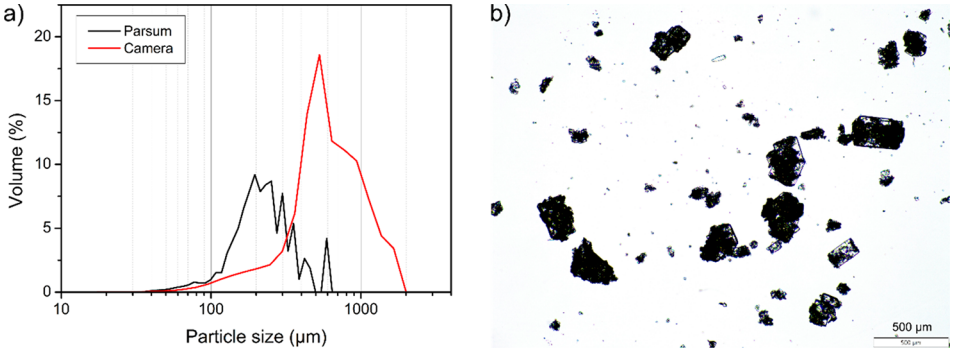

Figure 9. (a) Crystal size distribution and the (b) optical microscope image of the crystal sample taken at the third residence time of the continuous crystallization.

https://doi.org/10.1021/acs.oprd.1c00372
Org. Process Res. Dev. 2022, 26, 149−158

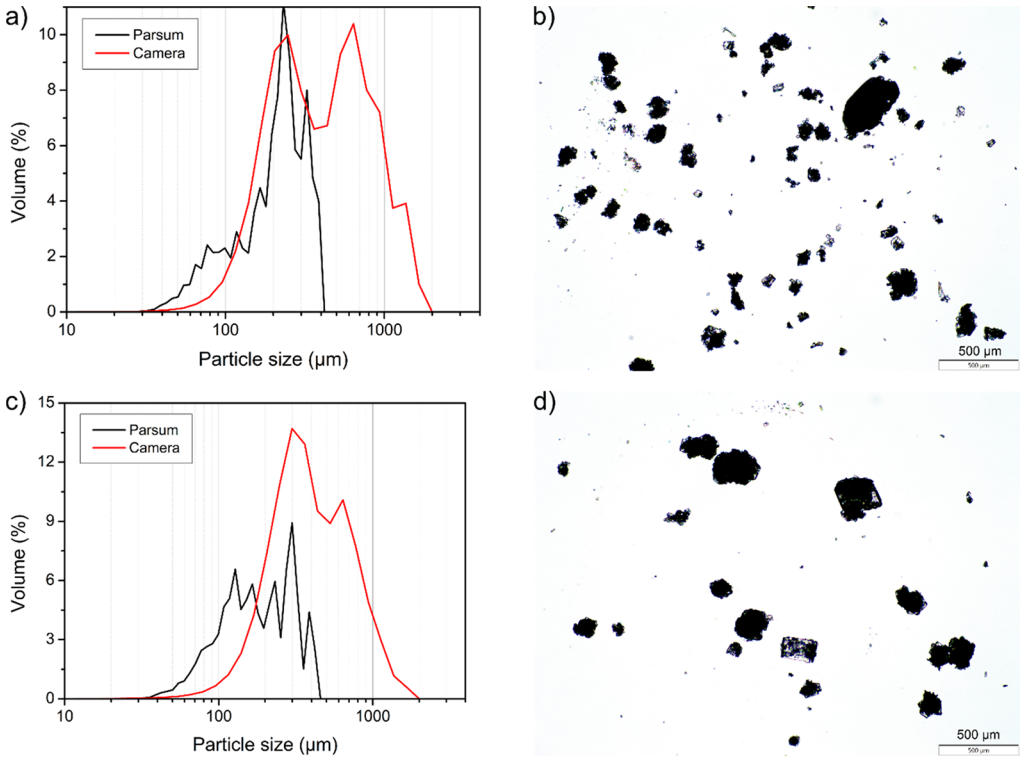

Figure 10. Crystal size distribution and the optical microscope image of the crystal sample taken at the (a, b) fourth and (c, d) fifth residence times of the continuous crystallization.

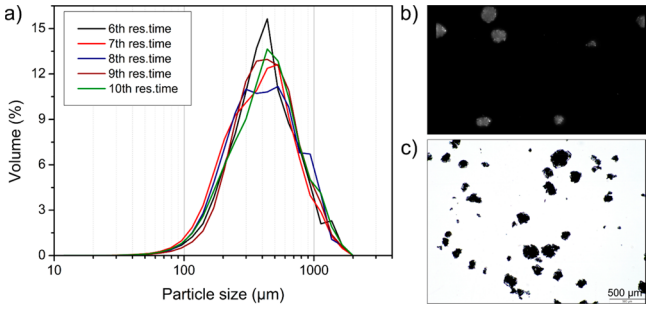

Figure 11. (a) Crystal size distributions, (b) an in-line captured image, and (c) an optical microscope image of the crystal sample from the steady state of the continuous crystallization (6th−10th residence times).

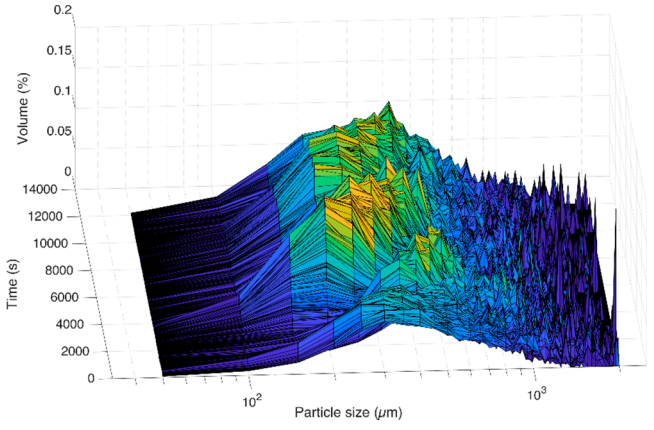

Figure 12. Result of continuous in-line image analysis of continuous MSMPR crystallization. A new CSD was calculated every 30 s from the detected crystals in the captured images.

available with this approach: approximately one million crystals were detected and measured within 3 min. We set the frequency of the new CSD calculation to 30 s, an interval that still contained much more data than a usual off-line particle size measurement. The calculated CSDs plotted against the elapsed time are presented in Figure 12.

At the beginning of the process, very broad CSDs were obtained, meaning that this period of the process was similarly challenging to monitor just like in the previous experiment. After the crystallization was initiated, crystal growth and agglomeration started in the system, which is clearly visible in Figure 12 from 2000 to 4000 s. Additionally, the width of the calculated distributions started to decrease soon after the start-up. After a certain size was reached, secondary nucleation was initiated, causing a major drop in mean crystal size at ∼5−6000 s. Shortly after, the process reached steady state with narrow and steady CSDs. The previously observed slight increase in the D_v50 values could be detected here as well. Altogether, the trends and events of the continuous crystallization process could be detected much more accurately and immediately after they occurred.

4. CONCLUSIONS

The continuous MSMPR crystallization of ASA was monitored in-line using image analysis in this work. The MSMPR reactor had overflow tubing for the outlet flow, which provided a unique, novel approach for the in-line monitoring of the process. A steep glass plate was placed under the tube, and a high-speed process camera was mounted in front of it. Several illumination arrangements were tested before the final light source and position were found, and a very short exposure time (250 μs) could be set, resulting in excellent quality, sharp crystal pictures. An image analysis software, developed in our

https://doi.org/10.1021/acs.oprd.1c00372
Org. Process Res. Dev. 2022, 26, 149−158

research group, was applied for the monitoring of the continuous crystallization of ASA. First, samples were taken for off-line analysis, and the camera was operated only during the sampling time interval. The result of the two methods showed similar trends in the process, but the different measurement principles resulted in different mean crystal sizes. The experiment was repeated by setting the same operating conditions to apply the image analysis for continuous process monitoring. This approach resulted in an enormous quantity of data, and the trends and events of the process could be detected and followed much more reliably and accurately. The developed method could provide a much easier tool for the quality control of the crystallizations than the currently available measurement techniques. In the future, we are planning to upgrade the imaging system as well as further develop the algorithm by implementing AI-based segmentation of the crystals.

AUTHOR INFORMATION

Corresponding Author

Panna Vass − *Budapest University of Technology and Economics, Department of Organic Chemistry and Technology, H-1111 Budapest, Hungary*; Phone: +36-1-463-1424; Email: panna.vass@oct.bme.hu

Authors

András Domokos − *Budapest University of Technology and Economics, Department of Organic Chemistry and Technology, H-1111 Budapest, Hungary*; orcid.org/0000-0003-1968-4679

Lajos Madarász − *Budapest University of Technology and Economics, Department of Organic Chemistry and Technology, H-1111 Budapest, Hungary*

György Stoffán − *Budapest University of Technology and Economics, Department of Organic Chemistry and Technology, H-1111 Budapest, Hungary*

Kornélia Tacsi − *Budapest University of Technology and Economics, Department of Organic Chemistry and Technology, H-1111 Budapest, Hungary*; orcid.org/0000-0001-8506-5062

Dorián Galata − *Budapest University of Technology and Economics, Department of Organic Chemistry and Technology, H-1111 Budapest, Hungary*

Kristóf Csorba − *Budapest University of Technology and Economics, Department of Automation and Applied Informatics, H-1111 Budapest, Hungary*

Zsombor K. Nagy − *Budapest University of Technology and Economics, Department of Organic Chemistry and Technology, H-1111 Budapest, Hungary*; orcid.org/0000-0003-2651-7756

Hajnalka Pataki − *Budapest University of Technology and Economics, Department of Organic Chemistry and Technology, H-1111 Budapest, Hungary*; orcid.org/0000-0002-8103-0601

Complete contact information is available at: https://pubs.acs.org/10.1021/acs.oprd.1c00372

Notes

The authors declare no competing financial interest.

ACKNOWLEDGMENTS

This work was supported by grants from the National Research, Development and Innovation Office of Hungary (grant numbers: KH-129584, FK-132133, PD-121143). The research reported in this paper and carried out at BME has been supported by the National Laboratory of Artificial Intelligence funded by the NRDIO under the auspices of the Ministry for Innovation and Technology. H.P. is thankful for the János Bolyai Research Scholarship of the Hungarian Academy of Sciences. Supported by the ÚNKP-21-3 and the ÚNKP-21-4-II New National Excellence Program of the Ministry for Innovation and Technology from the source of the National Research, Development and Innovation Fund.

REFERENCES

(1) Lee, S. L.; O'Connor, T. F.; Yang, X.; Cruz, C. N.; Chatterjee, S.; Madurawe, R. D.; Moore, C. M. V; Yu, L. X.; Woodcock, J. Modernizing Pharmaceutical Manufacturing: From Batch to Continuous Production. *J. Pharm. Innov.* **2015**, *10* (3), 191−199.

(2) Plumb, K. Continuous Processing in the Pharmaceutical Industry: Changing the Mind Set. *Chem. Eng. Res. Des.* **2005**, *83* (6), 730−738.

(3) Schaber, S. D.; Gerogiorgis, D. I.; Ramachandran, R.; Evans, J. M. B.; Barton, P. I.; Trout, B. L. Economic Analysis of Integrated Continuous and Batch Pharmaceutical Manufacturing: A Case Study. *Ind. Eng. Chem. Res.* **2011**, *50* (17), 10083−10092.

(4) Srai, J. S.; Harrington, T.; Alinaghian, L.; Phillips, M. Evaluating the Potential for the Continuous Processing of Pharmaceutical Products - A Supply Network Perspective. *Chem. Eng. Process.* **2015**, *97*, 248−258.

(5) Simon, L. L.; Pataki, H.; Marosi, G.; Meemken, F.; Hungerbühler, K.; Baiker, A.; Tummala, S.; Glennon, B.; Kuentz, M.; Steele, G.; Kramer, H. J. M.; Rydzak, J. W.; Chen, Z.; Morris, J.; Kjell, F.; Singh, R.; Gani, R.; Gernaey, K. V.; Louhi-Kultanen, M. J.; Sandler, N.; Antikainen, O.; Yliruusi, J.; Frohberg, P.; Ulrich, J.; Braatz, R. D.; Leyssens, T.; von Stosch, M.; Oliveira, R.; Tan, R. B. H.; Wu, H.; Khan, M. D.; Pandey, A.; Westra, R.; Delle-Case, E.; Pape, D.; Angelosante, D.; Maret, Y.; Steiger, O.; Lenner, M.; Abbou-Oucherif, K.; Nagy, Z. K.; Litster, J. D.; Kamaraju, V. K.; Chiu, M. S. Assessment of Recent Process Analytical Technology (PAT) Trends: A Multiauthor Review. *Org. Process Res. Dev.* **2015**, *19* (1), 3.

(6) Food and Drug Administration. *Guidance for Industry PAT: A Framework for Innovative Pharmaceutical Development, Manufacuring, and Quality Assurance*; FDA, 2004.

(7) Food and Drug Administration. *Quality Considerations for Continuous Manufacturing Guidance for Industry*; FDA, 2019.

(8) Chen, J.; Sarma, B.; Evans, J. M. B.; Myerson, A. S. Pharmaceutical Crystallization. *Cryst. Growth Des.* **2011**, *11* (4), 887−895.

(9) Borsos, Á.; Szilágyi, B.; Agachi, P. Ş.; Nagy, Z. K. Real-Time Image Processing Based Online Feedback Control System for Cooling Batch Crystallization. *Org. Process Res. Dev.* **2017**, *21* (4), 511−519.

(10) Blagden, N.; de Matas, M.; Gavan, P. T.; York, P. Crystal Engineering of Active Pharmaceutical Ingredients to Improve Solubility and Dissolution Rates. *Adv. Drug Delivery Rev.* **2007**, *59* (7), 617−630.

(11) Nagy, Z. K.; Fevotte, G.; Kramer, H.; Simon, L. L. Recent Advances in the Monitoring, Modelling and Control of Crystallization Systems. *Chem. Eng. Res. Des.* **2013**, *91* (10), 1903−1922.

(12) Silva, A. F. T.; Burggraeve, A.; Denon, Q.; Van Der Meeren, P.; Sandler, N.; Van Den Kerkhof, T.; Hellings, M.; Vervaet, C.; Remon, J. P.; Lopes, J. A.; De Beer, T. Particle Sizing Measurements in Pharmaceutical Applications: Comparison of in-Process Methods versus off-Line Methods. *Eur. J. Pharm. Biopharm.* **2013**, *85* (3 PART B), 1006−1018.

(13) Wong, S. Y.; Tatusko, A. P.; Trout, B. L.; Myerson, A. S. Development of Continuous Crystallization Processes Using a Single-Stage Mixed-Suspension, Mixed-Product Removal Crystallizer with Recycle. *Cryst. Growth Des.* **2012**, *12* (11), 5701−5707.

(14) Jiang, M.; Braatz, R. D. Designs of Continuous-Flow Pharmaceutical Crystallizers: Developments and Practice. *CrystEngComm* **2019**, *21* (23), 3534−3551.
(15) Su, Q.; Nagy, Z. K.; Rielly, C. D. Pharmaceutical Crystallisation Processes from Batch to Continuous Operation Using MSMPR Stages: Modelling, Design, and Control. *Chem. Eng. Process.* **2015**, *89*, 41−53.
(16) Agimelen, O. S.; Jawor-Baczynska, A.; McGinty, J.; Dziewierz, J.; Tachtatzis, C.; Cleary, A.; Haley, I.; Michie, C.; Andonovic, I.; Sefcik, J.; Mulholland, A. J. Integration of in Situ Imaging and Chord Length Distribution Measurements for Estimation of Particle Size and Shape. *Chem. Eng. Sci.* **2016**, *144*, 87−100.
(17) Agimelen, O. S.; Hamilton, P.; Haley, I.; Nordon, A.; Vasile, M.; Sefcik, J.; Mulholland, A. J. Estimation of Particle Size Distribution and Aspect Ratio of Non-Spherical Particles from Chord Length Distribution. *Chem. Eng. Sci.* **2015**, *123*, 629−640.
(18) Wang, X. Z.; Roberts, K. J.; Ma, C. Crystal Growth Measurement Using 2D and 3D Imaging and the Perspectives for Shape Control. *Chem. Eng. Sci.* **2008**, *63*, 1173.
(19) Gao, Z.; Wu, Y.; Bao, Y.; Gong, J.; Wang, J.; Rohani, S. Image Analysis for In-Line Measurement of Multidimensional Size, Shape, and Polymorphic Transformation of l -Glutamic Acid Using Deep Learning-Based Image Segmentation and Classification. *Cryst. Growth Des.* **2018**, *18* (8), 4275−4281.
(20) Zhou, Y.; Srinivasan, R.; Lakshminarayanan, S. Critical Evaluation of Image Processing Approaches for Real-Time Crystal Size Measurements. *Comput. Chem. Eng.* **2009**, *33* (5), 1022−1035.
(21) Ostergaard, I.; Szilagyi, B.; Nagy, Z. K.; de Diego, H. L.; Qu, H. Polymorphic Control and Scale-up Strategy for Crystallization from a Ternary Antisolvent System by Supersaturation Control. *Cryst. Growth Des.* **2020**, *20*, 1337.
(22) Simon, L. L.; Abbou Oucherif, K.; Nagy, Z. K.; Hungerbuhler, K. Bulk Video Imaging Based Multivariate Image Analysis, Process Control Chart and Acoustic Signal Assisted Nucleation Detection. *Chem. Eng. Sci.* **2010**, *65* (17), 4983−4995.
(23) Simon, L. L.; Nagy, Z. K.; Hungerbuhler, K. Endoscopy-Based in Situ Bulk Video Imaging of Batch Crystallization Processes. *Org. Process Res. Dev.* **2009**, *13* (6), 1254−1261.
(24) Jiang, M.; Braatz, R. D. Low-Cost Noninvasive Real-Time Imaging for Tubular Continuous-Flow Crystallization. *Chem. Eng. Technol.* **2018**, *41* (1), 143−148.
(25) Schorsch, S.; Ochsenbein, D. R.; Vetter, T.; Morari, M.; Mazzotti, M. High Accuracy Online Measurement of Multidimensional Particle Size Distributions during Crystallization. *Chem. Eng. Sci.* **2014**, *105*, 155−168.
(26) Cardona, J.; Ferreira, C.; Svoboda, V.; Ahmed, B.; McGinty, J.; Agimelen, O. S.; Hamilton, A.; Cleary, A.; Atkinson, R.; Michie, C.; et al. The Role of In-Line Image Analysis in the Transition to Continuous Manufacturing in the Pharmaceutical Industry. In *Advances in Manufacturing Technology XXXII*; IOS Press, 2018; Vol. 8, p 27; DOI: 10.3233/978-1-61499-902-7-27.
(27) Kempkes, M.; Eggers, J.; Mazzotti, M. Measurement of Particle Size and Shape by FBRM and in Situ Microscopy. *Chem. Eng. Sci.* **2008**, *63* (19), 4656−4675.
(28) Simone, E.; Saleemi, A. N.; Nagy, Z. K. In Situ Monitoring of Polymorphic Transformations Using a Composite Sensor Array of Raman, NIR, and ATR-UV/Vis Spectroscopy, FBRM, and PVM for an Intelligent Decision Support System. *Org. Process Res. Dev.* **2015**, *19* (1), 167−177.
(29) Abioye, A. O.; Chi, G. T.; Simone, E.; Nagy, Z. Real-Time Monitoring of the Mechanism of Ibuprofen-Cationic Dextran Crystanule Formation Using Crystallization Process Informatics System (CryPRINS). *Int. J. Pharm.* **2016**, *509* (1−2), 264−278.
(30) Venâncio, F.; Rosário, F.; Cajaiba, J. A Low-Cost System Based on Image Analysis for Monitoring the Crystal Growth Process. *Sensors* **2017**, *17* (6), 1248.
(31) Sarkar, D.; Doan, X. T.; Ying, Z.; Srinivasan, R. In Situ Particle Size Estimation for Crystallization Processes by Multivariate Image Analysis. *Chem. Eng. Sci.* **2009**, *64* (1), 9−19.
(32) Cardona, J.; Ferreira, C.; McGinty, J.; Hamilton, A.; Agimelen, O. S.; Cleary, A.; Atkinson, R.; Michie, C.; Marshall, S.; Chen, Y. C.; Sefcik, J.; Andonovic, I.; Tachtatzis, C. Image Analysis Framework with Focus Evaluation for in Situ Characterisation of Particle Size and Shape Attributes. *Chem. Eng. Sci.* **2018**, *191*, 208−231.
(33) El Arnaout, T.; Cullen, P. J.; Sullivan, C. A Novel Backlight Fiber Optical Probe and Image Algorithms for Real Time Size-Shape Analysis during Crystallization. *Chem. Eng. Sci.* **2016**, *149*, 42−50.
(34) El Arnaout, T.; Cullen, P. J. In Situ Image Processing and Data Binning Strategy for Particle Engineering Applications. *Chem. Eng. Technol.* **2020**, *43*, 1618−1629.
(35) Lu, Z.; Zhang, L.; Jiang, Y.; Zhang, C.; Zhang, G.; Liu, M. Crystal Morphology Monitoring Based on In-Situ Image Analysis of L-Glutamic Acid Crystallization. In *Proceedings of the 2019 International Conference on Computer, Network, Communication and Information Systems (CNCI 2019)*; Atlantis Press: Paris, France, 2019; DOI: 10.2991/cnci-19.2019.53.
(36) Borchert, C.; Temmel, E.; Eisenschmidt, H.; Lorenz, H.; Seidel-Morgenstern, A.; Sundmacher, K. Image-Based in Situ Identification of Face Specific Crystal Growth Rates from Crystal Populations. *Cryst. Growth Des.* **2014**, *14* (3), 952−971.
(37) Huo, Y.; Liu, T.; Yang, Y.; Ma, C. Y.; Wang, X. Z.; Ni, X. In Situ Measurement of 3D Crystal Size Distribution by Double-View Image Analysis with Case Study on L-Glutamic Acid Crystallization. *Ind. Eng. Chem. Res.* **2020**, *59* (10), 4646−4658.
(38) Kempkes, M.; Vetter, T.; Mazzotti, M. Measurement of 3D Particle Size Distributions by Stereoscopic Imaging. *Chem. Eng. Sci.* **2010**, *65* (4), 1362−1373.
(39) Neoptolemou, P.; Goyal, N.; Cruz-Cabeza, A. J.; Kiss, A. A.; Milne, D. J.; Vetter, T. A Novel Image Analysis Technique for 2D Characterization of Overlapping Needle-like Crystals. *Powder Technol.*, in press; DOI: 10.1016/j.powtec.2021.09.017.
(40) Schiele, S. A.; Antoni, F.; Meinhardt, R.; Briesen, H. Analysis of Nonideal Shape Evolution during Potash Alum Crystallization Using Microcomputed Tomography and Three-Dimensional Image Analysis. *Cryst. Growth Des.* **2021**, *21* (3), 1751−1761.
(41) Ferreira, A.; Faria, N.; Rocha, F.; Teixeira, J. A. Using an Online Image Analysis Technique to Characterize Sucrose Crystal Morphology during a Crystallization Run. *Ind. Eng. Chem. Res.* **2011**, *50* (11), 6990−7002.
(42) Schorsch, S.; Vetter, T.; Mazzotti, M. Measuring Multidimensional Particle Size Distributions during Crystallization. *Chem. Eng. Sci.* **2012**, *77*, 130−142.
(43) Chen, S.; Liu, T.; Xu, D.; Huo, Y.; Yang, Y. Image Based Measurement of Population Growth Rate for L-Glutamic Acid Crystallization. In *2019 Chinese Control Conference (CCC)*; IEEE, 2019; pp 7933−7938; DOI: 10.23919/ChiCC.2019.8866441.
(44) Manee, V.; Zhu, W.; Romagnoli, J. A. A Deep Learning Image-Based Sensor for Real-Time Crystal Size Distribution Characterization. *Ind. Eng. Chem. Res.* **2019**, *58* (51), 23175−23186.
(45) Wu, Y.; Lin, M.; Rohani, S. Particle Characterization with On-Line Imaging and Neural Network Image Analysis. *Chem. Eng. Res. Des.* **2020**, *157*, 114−125.
(46) Oliva, J. A.; Wu, W.-L.; Greene, M. R.; Pal, K.; Nagy, Z. K. Continuous Spherical Crystallization of Lysozyme in an Oscillatory Baffled Crystallizer Using Emulsion Solvent Diffusion in Droplets. *Cryst. Growth Des.* **2020**, *20* (2), 934−947.
(47) Oliva, J. A.; Pal, K.; Barton, A.; Firth, P.; Nagy, Z. K. Experimental Investigation of the Effect of Scale-up on Mixing Efficiency in Oscillatory Flow Baffled Reactors (OFBR) Using Principal Component Based Image Analysis as a Novel Noninvasive Residence Time Distribution Measurement Approach. *Chem. Eng. J.* **2018**, *351*, 498−505.
(48) Kacker, R.; Maaß, S.; Emmerich, J.; Kramer, H. Application of Inline Imaging for Monitoring Crystallization Process in a Continuous Oscillatory Baffled Crystallizer. *AIChE J.* **2018**, *64* (7), 2450−2461.
(49) Capellades, G.; Joshi, P. U.; Dam-Johansen, K.; Mealy, M. J.; Christensen, T. V.; Kiil, S. Characterization of a Multistage Continuous MSMPR Crystallization Process Assisted by Image

Analysis of Elongated Crystals. *Cryst. Growth Des.* **2018**, *18* (11), 6455−6469.
(50) Vancleef, A.; Maes, D.; Van Gerven, T.; Thomassen, L. C. J.; Braeken, L. Flow-through Microscopy and Image Analysis for Crystallization Processes. *Chem. Eng. Sci.* **2022**, *248*, 117067.
(51) Madarász, L.; Nagy, Z. K.; Hoffer, I.; Szabó, B.; Csontos, I.; Pataki, H.; Démuth, B.; Szabó, B.; Csorba, K.; Marosi, G. Real-Time Feedback Control of Twin-Screw Wet Granulation Based on Image Analysis. *Int. J. Pharm.* **2018**, *547* (1−2), 360−367.
(52) Madarász, L.; Köte, Á.; Gyürkés, M.; Farkas, A.; Hambalkó, B.; Pataki, H.; Fülöp, G.; Marosi, G.; Lengyel, L.; Casian, T.; Csorba, K.; Nagy, Z. K. Videometric Mass Flow Control: A New Method for Real-Time Measurement and Feedback Control of Powder Micro-Feeding Based on Image Analysis. *Int. J. Pharm.* **2020**, *580*, 119223.
(53) Tacsi, K.; Pataki, H.; Domokos, A.; Nagy, B.; Csontos, I.; Markovits, I.; Farkas, F.; Nagy, Z. K.; Marosi, G. Direct Processing of a Flow Reaction Mixture Using Continuous Mixed Suspension Mixed Product Removal Crystallizer. *Cryst. Growth Des.* **2020**, *20* (7), 4433−4442.
(54) Domokos, A.; Nagy, B.; Gyürkés, M.; Farkas, A.; Tacsi, K.; Pataki, H.; Liu, Y. C.; Balogh, A.; Firth, P.; Szilágyi, B.; Marosi, G.; Nagy, Z. K.; Nagy, Z. K. End-to-End Continuous Manufacturing of Conventional Compressed Tablets: From Flow Synthesis to Tableting through Integrated Crystallization and Filtration. *Int. J. Pharm.* **2020**, *581*, 119297.
(55) Balogh, A.; Domokos, A.; Farkas, B.; Farkas, A.; Rapi, Z.; Kiss, D.; Nyiri, Z.; Eke, Z.; Szarka, G.; Örkényi, R.; Mátravölgyi, B.; Faigl, F.; Marosi, G.; Nagy, Z. K. Continuous End-to-End Production of Solid Drug Dosage Forms: Coupling Flow Synthesis and Formulation by Electrospinning. *Chem. Eng. J.* **2018**, *350*, 290−299.
(56) Bradski, G. References. *Lang. Learn.* **2000**, *50*, 439−461.
(57) Kelly, K. E.; Whitaker, J.; Petty, A.; Widmer, C.; Dybwad, A.; Sleeth, D.; Martin, R.; Butterfield, A. Ambient and Laboratory Evaluation of a Low-Cost Particulate Matter Sensor. *Environ. Pollut.* **2017**, *221*, 491−500.
(58) Folttmann, F.; Knop, K.; Kleinebudde, P.; Pein, M. In-Line Spatial Filtering Velocimetry for Particle Size and Film Thickness Determination in Fluidized-Bed Pellet Coating Processes. *Eur. J. Pharm. Biopharm.* **2014**, *88* (3), 931−938.

https://doi.org/10.1021/acs.oprd.1c00372
Org. Process Res. Dev. 2022, 26, 149−158